FABRICATION OF SUBMICRON TUNABLE METAMATERIAL INFRARED ABSORBERS FOR GAS SENSING USING OPTICAL CONTACT LITHOGRAPHY

Amirali Nikeghbal, Md Rabiul Hasan, Adwait Deshpande, Fatemeh Momeni, Seungbeom Noh, Hanseup Kim, and Carlos H. Mastrangelo
University of Utah, Salt Lake City, USA

ABSTRACT

A standard method for discriminating a gas mixture utilizes gas-specific infrared (IR) absorbance. Due to their structural simplicity and tunability, the spectrum of the gas IR transmission signature is measured with a set of tunable IR filters of metamaterial absorbers (MMA). However, the fabrication of MMAs requires expensive sub-micron lithography. This paper presents a low-cost method for fabricating MMAs with submicron features utilizing inexpensive contact lithography. The patterning method uses a silicon nitride (SiN) membrane with micron-sized openings that shrink to submicron dimensions by conformal deposition of SiN. The resulting holey membrane is used as a submicron shadow mask to define metal patterns on MMAs. Using this technique, we demonstrated the low-cost fabrication and test of MMAs in the 2-7 μm IR range and also openings down to 380 nm diameter and transferred patterns down to 480 nm.

KEYWORDS

Metamaterial, Infra-red absorber, Contact Lithography.

INTRODUCTION

Metal-insulator-metal metamaterial absorbers, which are synthetic nanostructures made up of complicated arrangements of metallic patterns and stacked dielectric, because of their unique capacity to provide highly effective near-unity absorption within a small frequency range [1], and also due to the ease of design, have been used extensively to implement tunable optical [2], near, mid, and long-infrared [3]-[6] filters and absorbers. Generally, metamaterial absorbers ranging from microwaves [7], and terahertz to optical frequencies have attracted much attention recently. Metamaterials' absorption and emission characteristics, including central resonant frequency and full-width at half maximum, are heavily influenced by their geometry, hence adjusting the size, periodicity, and shape of subwavelength elements allows one to tune the amplitude and frequency of the electromagnetic radiation's electric [$\epsilon(\omega)$] and magnetic [$\mu(\omega)$] responses [8]. Metamaterial absorbers are categorized into two different classes, usually based on their functionality in processing the Electromagnetic wave that interacts with them: sharp resonant absorbers, which provide absorption at specific resonant frequencies, and broadband absorbers that have an extensive absorption over a wavelength or frequency domain for instance, S. Kang, et al.[5] showcased ultra-narrow band absorption, while F. Ding et al. [3] documented similarly broad-band MMAs.

A great number of optical and photonic component device-based phenomena have used metasurfaces, such as efficient flat lenses and smart contact lenses, which have the potential to integrate metamaterials in various ways to enhance their functionality and capabilities. As a result, metamaterials can dramatically enhance the properties inside smart contact lenses [9]-[13]. Also, a combination of a metamaterial IR absorber and a Microbolometer IR absorber, due to the bandwidth tuning capability of metamaterial, can help enhance the performance and functionality of IR Microbolometer sensing systems by improving the detection sensitivity, spectral selectivity, and polarization sensitivity and as miniaturization can be achieved [14]-[19]. Overall, metamaterials offer promising prospects for a wide range of optical photovoltaic devices [20], tunable biochemical sensors [21], [22], low power gas sensors[23], and solar cells [24].

A pervasive issue that limits the utilization of metamaterial filters is their needs for very fine patterns which are much smaller than the wavelength of the light filtered. Typical pattern dimensions range from λ/2 to λ/10; hence, fabrication requires high-cost submicron nanolithography and electron beam lithography followed by lift-off techniques [5], [25][26].

In this paper we present a novel cost-effective sub micrometer patterning method for metamaterial filters that utilizes conventional optical contact lithography followed by isotropic feature shrinkage. We designed and fabricated infrared MMAs of the type depicted in Fig. 1 utilizing this technique with <0.5 μm feature size.

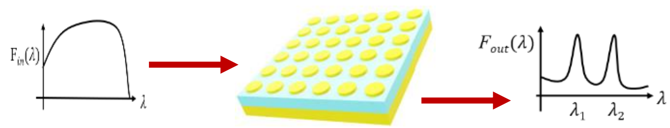

Figure 1. Demonstration of the array of metamaterial absorber and working principle for absorbing some portion of a broad band IR radiation.

DESIGN AND EQUIVALENT CIRCUIT MODEL

In order to interpret the mechanism and theory of metamaterials, different theories have been proposed, such as the interference theory [27], transmission line theory [28], and coupled mode theory [29]. By using the resistor-inductor-capacitor (RLC) circuit model the magnetic resonances and polarization inside the metastructures can be described. The RLC circuit model predicts the resonance frequency, the full width at half maximum, and the quality factor for different geometric designs [30]-[32].

The permittivity and permeability of the material used in MMAs play a crucial role in determining resonant frequency, and it has already been explored that a nanosphere material with positive real part permittivity can be considered a nano-capacitor and a negative sign of the real part of permittivity of a nanosphere material is considered nano-inductance [30]. On the other hand, any values for the imaginary part of the permittivity lead to the resistivity loss and count as a nano-resistor, thus, a proper arrangement of materials with different signs of the real part of permittivity can tune the local electric field, and one can provide functionality for information processing like low-pass, high-pass, or band-pass filtering of the signals by using parallel or series combination of these negative and positive real part permittivity materials to make RLC filter circuits [31]. Hence, the frequency response of these MMAs is modeled with a few equivalent circuit components [32]. Fig. 2a demonstrates the equivalent circuit model for the MIM-MMA. As shown in Fig. 2b the top layer of the single cell structure is a metal with Real ($\boldsymbol{\epsilon}$) < 0 thus modeled as an inductance called resonant inductance (L_r); Due to the metal loss ($\mathrm{Im}(\boldsymbol{\epsilon}) \neq 0$) we need to consider a resistor (R_r) in series with L_r; The SiO_2 dielectric, between resonator gold dots and ground plane gold mirror, due to the material property of Real ($\boldsymbol{\epsilon}$) > 0, is modeled as a nano-capacitor (C_d); Analogous to top resonator, for ground plane gold mirror we have a nano-inductance (L_g) and a nano-resistor (R_g). Moreover, the effect of mutual inductances between bottom gold mirror plane and top resonator is also considered as L_m. Finally, the air-gap between each resonator single cell is considered as capacitor C_p as the air have a Real (**ϵ**) > 0 property. A. Sakurai et.al, [32] mentioned that circuit equivalents work approximately for designing desired values for desire wavelengths, they derived the following equations for L_r, L_g, L_m, R_g, R_r, C_d, and C_p, to predict the resonant wavelength of the structures that are smaller than the incident radiation wavelength [33], [34], where **δ** is penetration depth (nm), **ω** is the frequency (Hz), **ϵ_0** is permittivity of vacuum (8.854×10^{-12} F/m), **ϵ** is the dielectric function of metal ($\epsilon = \epsilon' + i\epsilon''$), and constant factor of c is a compensator for the non-uniform charge distribution along the capacitor surfaces ranging 0.4-0.5.

$$L_m = \frac{\mu_0 w d}{2l} \quad (1)$$

$$L_r = -\frac{w}{l\epsilon_0\omega^2\delta}\left(\frac{\epsilon'}{\epsilon'^2+\epsilon''^2}\right) \quad (2)$$

$$L_g = -\frac{1}{\epsilon_0\omega^2\delta}\left(\frac{\epsilon'}{\epsilon'^2+\epsilon''^2}\right) \quad (3)$$

$$R_r = -\frac{w}{l\epsilon_0\omega\delta}\left(\frac{\epsilon''}{\epsilon'^2+\epsilon''^2}\right) \quad (4)$$

$$R_g = -\frac{1}{\epsilon_0\omega\delta}\left(\frac{\epsilon''}{\epsilon'^2+\epsilon''^2}\right) \quad (5)$$

$$C_d = \frac{c\epsilon_d\epsilon_0 wl}{d} \quad (6)$$

$$C_p = \frac{\epsilon_0 hl}{P-w} \quad (7)$$

$$Z_{tot}(\omega) = R_r + R_g + \frac{2}{j\omega C_d} + j\omega(L_g + L_r) + 2j\omega L_m \quad (8)$$

For the maximum absorption (A) and minimize the reflection (**Γ**), the Z_{tot} needs to be equal to free space impedance (Z_0 ~377**Ω**):

$$|\Gamma|^2 = \left|\frac{Z_{tot} - Z_0}{(Z_{tot}+Z_0)}\right|^2 \quad (9)$$

Finally, the resonant frequency is estimated by zeroing the total impedance, for simple calculation the effect of C_p is ignored:

$$f_r = \sqrt{\frac{2}{(2L_m+L_r+L_g)C_d}} \quad (10)$$

The Quality Factor (QF) of each filter can be achieved by dividing the Central frequency over FWHM.

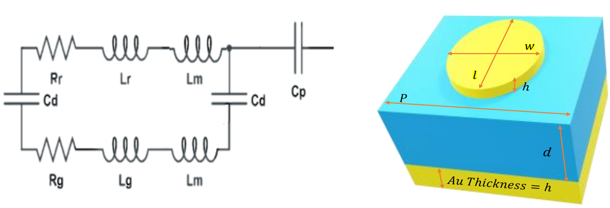

(a) *(b)*

Figure 2: (a) Equivalent circuit model of metamaterial, (b) Metamaterial single cell structure

FABRICATION

The Metal Insulator Metal Metamaterial Absorber (MIM-MMA) consist of three main layers: a bottom metal layer, a middle dielectric layer, and a top periodic metal micro patch dots; Our new MMA patterning method utilizes a shrinkable shadow mask of micrometer dimensions fabricated with conventional low-cost optical lithography. The shadow mask openings are shrunk to submicron dimensions via conformal deposition. Fig. 3a shows the process flow for creating the sub-micron shadow mask. This innovative high-resolution and tunable shadow mask aims to eliminate the high cost of using nanolithography and EBL to pattern sub-micron feature sizes. In this method, a thick layer of 800 nm Silicon Nitride was first deposited using an LPCVD furnace on a prime p-type (100) orientation silicon wafer. Next, the nitride on the top side was patterned in the range of 1-2 micrometers in different hole sizes using the conventional photolithography method and CF4/O2 RIE to reach the surface of the Si substrate. Next, the wafer was returned to the nitride furnace, followed by another 400nm LPCVD SiN deposition to 1) Fill in the etched holes and shrink the features to the desired dimensions, 2) Create an etch stop membrane which works as a passivation layer on the top side against the incoming KOH wet etching step [35]. Next, the backside silicon nitride is etched using RIE. The silicon under the top SiN is next etched with a 40% KOH solution at 70°C until the top silicon nitride layer was reached, thus, forming a thin suspended membrane. After rinsing and drying, the wafer was again blanket etched with C4/O2 to create through holes in the membrane in a net-like surface on a 300µm × 300µm footprint. After this step, another precise 400nm LPCVD Si_3N_4 deposition step followed, which reduced the hole diameters to sub-micron dimensions. Using this method, we were able to create openings down to 380 nm diameter. Fig. 3b describes the process flow for fabricating the MMAs. 10nm Ti and 100nm Au were sputtered on a silicon substrate which acts as a non-transmitted layer for Infra-Red incident [5]. This was followed by a 200nm RF sputtered SiO2 dielectric layer. The fabricated sub-micron shadow mask was flipped and attached to this wafer and 100nm gold was evaporated through it to form sub-micron Au dot patterns.

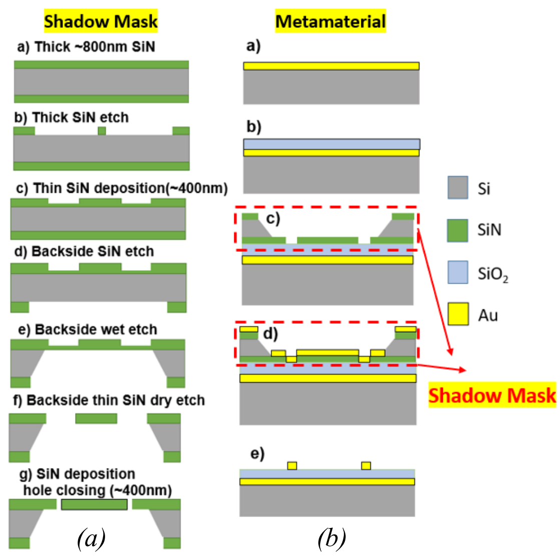

(a) *(b)*

*Figure 3: **a)** Fabrication process flow of the Shadow Mask and **b)** MIM Metamaterial absorber.*

RESULTS AND DISSCUTION

We fabricated seven filters with Au-dot feature sizes ranging from 0.4 to 1.4µm, as shown in table 1 and 2. Fig. 4a shows SEM images of the sub-micron shadow mask holes with different sizes in which the secondary grown S_3N_4 is clearly distinguishable from the original thick nitride. In Fig. 4b the resulting different size Au dots for the MMAs are demonstrated. The patterned dots range from 480 nm to 1.4 um. There is a deviation factor of about 15-25% between the through hole size and the final size of the patterned dot, which can be improved by reducing the gap between shadow mask and substrate during E-beam Evaporation. An array part of the full 300 × 300 um footprint of the both shadow mask and MMAs are depicted in Fig. 4c and 4d. For instance, the resulting 400 nm opening initially was a 2000 nm hole, and after a total of 800 nm SiN deposition during two deposition steps, it was achieved. The same technique with different deposition thicknesses used to achieve holes of different sizes. Since the deposition is isotropic, the shrinkage rate is doubled at the end. Table 1 describes the initial and final diameter for some of the holes after 800 and 500 nm SiN deposition. It worth mentioning that due to inherent LPCVD furnace limit, the deposition is not always exact and uniform resulting in about 5% deviation in between the expected and actual final diameter of holes, after the SiN deposition.

Table 1: Initial patterned hole diameter (D_i) and final targeted internal diameter (D_f) of opening holes in the shadow mask after the isotropic deposition of SiN for shrinking.

D_i (nm)	Total Deposition (nm)	D_f (nm)
2000	800	400
2400	800	800
2500	800	900
2100	500	1100
2300	500	1300
2400	500	1400

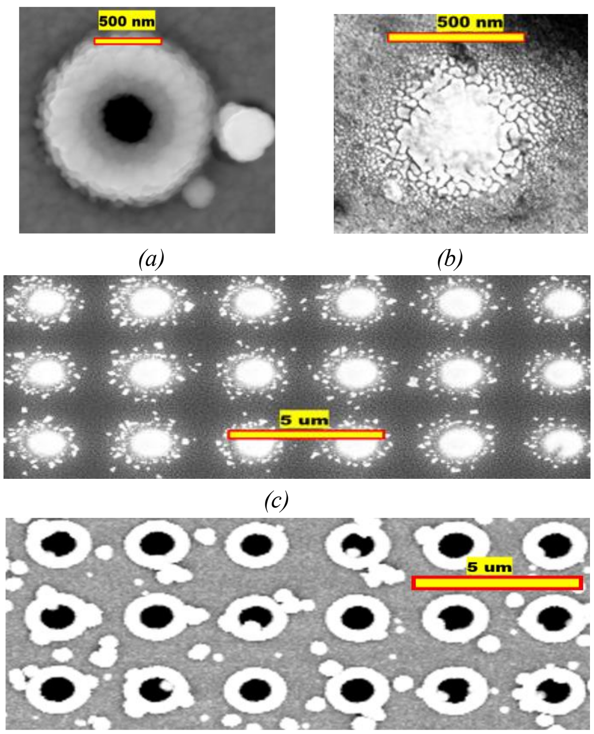

(d)

Figure 4: SEM images of different size holes and gold dots (a) through hole on the thick membrane of shadow mask (b) final patterned single cell submicron feature (c) patterned meta dot array and (d) Shadow mask through holes array.

In Fig. 5, the experimental results of the infrared incident absorption of different-sized metamaterial absorbers are illustrated. These findings highlight the remarkable, precise, and tunable patterning power of our fabrication method, as well as the efficacy of the membrane-meshed shadow mask for producing practical wavelength-selective metamaterial absorbers. Absorption measurements were conducted within the 2–8 µm wavelength range. A Fourier-transform infrared spectrometer with a liquid-N2-cooled infrared microscope was used to quantify transmission and reflection of each device. The absorption is then computed using the observed transmission and reflection using A = 1-R-T equation. Due to the fact that the bottom Au layer (100 nm Au) of the fabricated absorbers is thicker than the penetration depth of Gold ($\delta Au \approx 20nm$) at the working IR wavelengths, we can ignore the transmission ($T \approx 0$) [36]. Fig. 5 depicts the Absorption versus Wavelength plots related to different dimensions mentioned in table 2. As presented in the table 2, 7 circle-shape structures with the diameter ranging from 0.4 to 1.4 um have been fabricated which each one has its own wavelength-specific absorption.

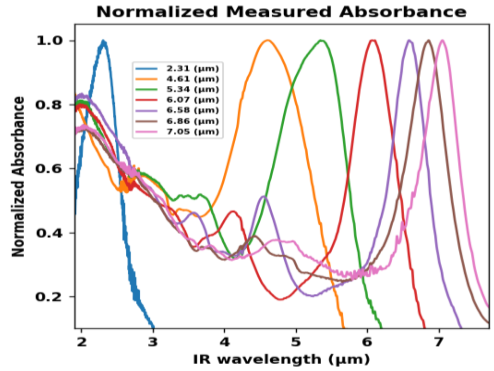

Figure 5: Experimentally Absorption measurement of different Metamaterial devices.

Table 2: lateral dimensions (Diameter and Periodicity) with respect to the experimentally measured peak absorption wavelength (λ_{peak}), Full-Width at Half-Maximum, and Quality Factor of the 7 different size Metamaterial IR absorbers.

#	Lateral Dimension		Spectral Characteristics			
	w (µm)	*P* (µm)	*Wavelength Peak* (µm)	*Abs* (%)	*QF*	*FWHM* (um)
1	0.4	2.8	2.31	~25	2.6	0.772
2	0.8	2.8	4.61	~50	3.3	1.3
3	0.9	2.8	5.34	~70	4.5	1.2
4	1.1	2.8	6.07	~85	7.6	0.800
5	1.2	2	6.58	~86	10.3	0.639
6	1.3	2	6.86	~82	9	0.764
7	1.4	2	7.05	~86	9.7	0.724

CONCLUSION

In this work, we introduced a novel and precise patterning method to fabricate submicron feature sizes using conventional and optical lithography techniques. By using a tunable shadow mask technique, we represented significant progress in the microfabrication field, as it is a cost-effective alternative and much more accessible than the nano-lithography or EBL methods. To evaluate our method, we successfully manufactured seven metamaterial infrared absorbers, which previously had been fabricated by using nano or electron beam lithography. It is worth mentioning that the infrared absorbers fabricated using our technique exhibited an average quality factor of 6.7. These results provide a potential road to enable the bulk fabrication of high-quality metamaterial devices for various applications in IR-sensing, Imaging, Optics, Biomedical, etc.

ACKNOWLEDGEMENTS

All of the fabrication steps were performed at the state-of-art Utah Nano Fabrication Laboratory Facility, Salt Lake City, Utah, USA, also thanks to the DOE ARPA-E grant 55801019 which supported us to complete this research.

REFERENCES

[1] N. Liu, M. Mesch, T. Weiss, M. Hentschel, and H. Giessen, "Infrared perfect absorber and its application as plasmonic sensor," *Nano Lett.*, vol. 10, no. 7, pp. 2342–2348, 2010.

[2] J. A. Bossard, L. Lin, S. Yun, L. Liu, D. H. Werner, and T. S. Mayer, "Near-Ideal Optical Metamaterial

Bandwidth," *ACS Nano*, vol. 8, no. 2, pp. 1517–1524, 2014.
[3] F. Ding, J. Dai, Y. Chen, J. Zhu, Y. Jin, and S. I. Bozhevolnyi, "Broadband near-infrared metamaterial absorbers utilizing highly lossy metals," *Sci. Rep.*, vol. 6, no. June, pp. 1–9, 2016.
[4] X. Liu, T. Starr, A. F. Starr, and W. J. Padilla, "Infrared spatial and frequency selective metamaterial with near-unity absorbance," *Phys. Rev. Lett.*, vol. 104, no. 20, pp. 1–4, 2010.
[5] S. Kang, "Ultra-narrowband Metamaterial Absorbers for Multispectral Infrared Microsystems," no. December, 2018.
[6] X. Zhao, C. Chen, A. Li, G. Duan, and X. Zhang, "Implementing infrared metamaterial perfect absorbers using dispersive dielectric spacers," *Opt. Express*, vol. 27, no. 2, p. 1727, 2019.
[7] F. Ding, Y. Cui, X. Ge, Y. Jin, and S. He, "Ultra-broadband microwave metamaterial absorber," *Appl. Phys. Lett.*, vol. 100, no. 10, pp. 1–5, 2012.
[8] C. M. Watts, X. Liu, and W. J. Padilla, "Metamaterial electromagnetic wave absorbers," *Adv. Mater.*, vol. 24, no. 23, 2012.
[9] M. Khorasaninejad, W. T. Chen, R. C. Devlin, J. Oh, A. Y. Zhu, and F. Capasso, "Metalenses at visible wavelengths: Diffraction-limited focusing and subwavelength resolution imaging," *Science (80-.).*, vol. 352, no. 6290, pp. 1190–1194, 2016.
[10] C. Ghosh *et al.*, "Artificial Iris on Smart Contact Lens using Twisted Nematic Cell for Photophobia Alleviation," *2023 IEEE Photonics Conf. IPC 2023 - Proc.*, no. 1, pp. 1–2, 2023.
[11] A. Deshpande *et al.*, "Automatic Light Intensity Modulation Using TNC-based Artificial Iris for Smart Contact Lens," *Proc. IEEE Sensors*, pp. 1–4, 2023.
[12] A. Banerjee *et al.*, "Refractive-type varifocal liquid-crystal Fresnel lenses for smart contacts," *Opt. Express*, vol. 31, no. 10, p. 17027, 2023.
[13] C. Ghosh *et al.*, "Flexible, Refractive Fresnel Liquid-Crystal (RFLC) Lens for Low-Power Autofocusing Smart Contact Lens Systems," *2023 Conf. Lasers Electro-Optics, CLEO 2023*, no. 1, pp. 9–10, 2023.
[14] E. Information, Y. Raytron, and T. Company, "Metamaterial microbolometers for multi-spectral infrared polarization imaging," vol. 30, no. 6, pp. 9065–9087, 2022.
[15] J. Grant, I. Escorcia-carranza, C. Li, I. J. H. Mccrindle, J. Gough, and D. R. S. Cumming, "PAPER A monolithic resonant terahertz sensor element comprising a metamaterial absorber and micro-bolometer," vol. 1048, no. 6, pp. 1043–1048.
[16] M. Daneshnazar, B. Jaleh, M. Eslamipanah, and R. S. Varma, "Optical and gas sensing properties of TiO2/RGO for methanol, ethanol and acetone vapors," *Inorg. Chem. Commun.*, vol. 145, no. September, p. 110014, 2022.
[17] M. Hasan *et al.*, "Wavelength-Skewed Microbolometer Arrays," *2023 IEEE SENSORS*, vol. 1, pp. 1–4.
[18] A. Nasri, B. Jaleh, M. Daneshnazar, and R. S. Varma, "Sensing Properties of g-C3N4/Au Nanocomposite for Organic Vapor Detection," *Biosensors*, vol. 13, no. 3, 2023.
[19] M. R. Hasan et al., "High-Responsivity Vacuum less Microbolometer Arrays Microfabricated on Thermally Isolated Suspended Membranes," Proc. IEEE Int. Conf. Micro Electro Mech. Syst., no. January, pp. 1047–1050, 2024.
[20] E. Zamani, M. Malekmohammad, and A. Taherian, "External pumped all-optical microfiber modulator based on reduced graphene oxide," *Appl. Opt.*, vol. 62, no. 5, p. 1376, 2023.
[21] M. M. Hassan, F. S. Sium, F. Islam, and S. M. Choudhury, "A review on plasmonic and metamaterial based biosensing platforms for virus detection," *Sens. Bio-Sensing Res.*, vol. 33, no. May, p. 100429, 2021.
[22] B. Wang, C. Xu, G. Duan, W. Xu, and F. Pi, "Review of Broadband Metamaterial Absorbers : From Principles , Design Strategies , and Tunable Properties to Functional Applications," vol. 2213818, pp. 1–58, 2023.
[23] A. Lochbaum *et al.*, "Compact Mid-Infrared Gas Sensing Enabled by an All-Metamaterial Design," 2020.
[24] Y. Wang, T. Sun, T. Paudel, Y. Zhang, Z. Ren, and K. Kempa, "Metamaterial-Plasmonic Absorber Structure for High Efficiency Amorphous Silicon Solar Cells," 2012.
[25] U. Huebner, M. Falkner, U. D. Zeitner, M. Banasch, K. Dietrich, and E.-B. Kley, "Multi-stencil character projection e-beam lithography: a fast and flexible way for high quality optical metamaterials," *30th Eur. Mask Lithogr. Conf.*, vol. 9231, p. 92310E, 2014.
[26] Y. Chen, "Nanofabrication by electron beam lithography and its applications: A review," *Microelectron. Eng.*, vol. 135, pp. 57–72, 2015.
[27] H. Chen, "Interference theory of metamaterial perfect absorbers," vol. 20, no. 7, pp. 7165–7172, 2012.
[28] A. Rastgordani, Z. Ghattan Kashani, and M. S. Abrishamian, "A general equivalent circuit model for plasmonic metasurface broadband absorbers," *Optik (Stuttg).*, vol. 221, no. March, p. 165354, 2020.
[29] L. Zhu, S. Sandhu, C. Otey, S. Fan, M. B. Sinclair, and T. S. Luk, "Temporal coupled mode theory for thermal emission from a single thermal emitter supporting either a single mode or an orthogonal set of modes," *Appl. Phys. Lett.*, vol. 102, no. 10, 2013.
[30] N. Engheta, A. Salandrino, and A. Alu, "Circuit Elements at Optical Frequencies : Nanoinductors , Nanocapacitors , and Nanoresistors," vol. 095504, no. August, pp. 1–4, 2005.
[31] N. Engheta, "Circuits with light at nanoscales: Optical nanocircuits inspired by metamaterials," *Science (80-.).*, vol. 317, no. 5845, pp. 1698–1702, 2007.
[32] A. Sakurai, B. Zhao, and Z. M. Zhang, "Prediction of the Resonance Condition of Metamaterial Emitters and Absorbers Using LC Circuit Model," no. August 2014, 2014.
[33] A. Sakurai, B. Zhao, and Z. M. Zhang, "Resonant frequency and bandwidth of metamaterial emitters and absorbers predicted by an RLC circuit model," *J. Quant. Spectrosc. Radiat. Transf.*, vol. 149, pp. 33–40, 2014.
[34] Solymar L, Shamonina E. Waves in metamaterials. Oxford: Oxford University Press; 2009.
[35] E. Pourshaban *et al.*, "Power Scavenging Microsystem for Smart Contact Lenses," *Small*, vol. 2401068, pp. 1–8, 2024.
[36] R. L. Olmon *et al.*, "Optical dielectric function of gold," no. December, 2012.

CONTACT

*A.N. Public, tel: +1-385-458-6112; amirali.nikeghbal@utah.edu